

Chaotic dynamics of Bose-Einstein condensate in a density-dependent gauge field

Lei Chen^{1,2} and Qizhong Zhu^{1,3,*}

¹*Guangdong Provincial Key Laboratory of Quantum Engineering and Quantum Materials,
School of Physics and Telecommunication Engineering,
South China Normal University, Guangzhou 510006, China*

²*School of Physics and Electronic Science, Zunyi Normal University, Zunyi 563006, China*

³*Guangdong-Hong Kong Joint Laboratory of Quantum Matter,
Frontier Research Institute for Physics, South China Normal University, Guangzhou 510006, China*

(Dated: November 23, 2021)

In this work we study the effect of density-dependent gauge field on the collective dynamics of a harmonically trapped Bose-Einstein condensate, beyond the linear response regime. The density-dependent gauge field, as a backaction of the condensate, can in turn affect the condensate dynamics, resulting in highly nonlinear equations of motion. We find that the dipole and breathing oscillations of the condensate along the direction of gauge field are coupled by this field. For a quasi-one-dimensional condensate, this coupling makes the collective motion quasiperiodic. While for a quasi-two-dimensional condensate, the gauge field can also induce a Hall effect, manifested as an additional coupling between dipole and breathing oscillations in perpendicular direction. When the density-dependent gauge field is strong, the interplay between these oscillations can cause the collective dynamics of the condensate to become chaotic. Our findings reveal an important effect of dynamical gauge field on the nonlinear dynamics of a Bose-Einstein condensate.

I. INTRODUCTION

The emulation of gauge field in cold atomic gases is one of the major topics attracting persistent interest. Significant progress has been made in the engineering of artificial gauge field in the last decades, including both the abelian [1–4] and non-abelian gauge field, in particular, the spin-orbit coupling [4–10]. Nevertheless, most research has previously mainly focused on the realization of a static gauge field, where the generated artificial gauge field is completely determined by the external laser field, and itself has no dynamics. Recently, simulating dynamical gauge field in cold atoms has gained increasing interest and attention in the community. Until now, a variety of theoretical proposals to create dynamical gauge field have been put forward and some already been experimentally realized [11–22]. Those schemes either exploit the quantum nature of external control light, or make the gauge field dependent on the atomic density. It is an important and interesting topic to explore the new physics brought by those dynamical gauge fields [23–27].

One prominent effect induced by a static gauge field, e.g., the magnetic field, is the celebrated Hall effect for electrons in solids. For cold neutral gases, a superfluid can also exhibit Hall effect, when subject to an static artificial magnetic field [28–30]. Will the dynamical gauge field also induce a Hall effect on the transverse motion of a condensate? If true, how will the collective dynamics of the condensate influenced by the Hall effect?

In this paper, we try to address these issues by considering dynamical gauge field which depends on the atomic density [15]. Previous studies on the effect of density-

dependent gauge field mainly focus on the quasi-one-dimensional (quasi-1D) case [15, 31–33] and vortex related physics in quasi-two-dimensional (quasi-2D) case [34, 35]. To explore physics like Hall effect, the condensate dynamics has to be treated as quasi-2D. In particular, we study the effect of density-dependent gauge field on the collective dynamics of a Bose-Einstein condensate (BEC) confined in a harmonic trap, beyond the linear response regime. We find that, in quasi-1D case, the dipole and breathing oscillations in the direction of gauge field are coupled, resulting in quasiperiodic motion of these modes, even when the gauge field is quite strong. While in quasi-2D case, these two modes are additionally coupled with the breathing oscillation in the perpendicular direction through the Hall effect, and their interplay can lead to a chaotic dynamics in the presence of a strong gauge field. Our findings shed light on the intriguing effect of dynamical gauge field on the nonlinear dynamics of BEC.

This paper is organized as follows. First, in Sec. II we employ the variational wave function method to derive the coupled motion of center of mass and width, namely, the dipole mode and breathing mode of a BEC, and arrive at a set of nonlinear equations. We then solve these coupled equations numerically, with results presented in Sec. III, and investigate the nature of the condensate dynamics, namely, regular or chaotic. This is demonstrated by computing the Poincaré section, both in four-dimensional (4D) form and its 2D projection [36], along with the analysis of power spectrum of the dynamical variables. Finally, we end our discussion with a summary in Sec. IV.

* qzzhu@m.scnu.edu.cn

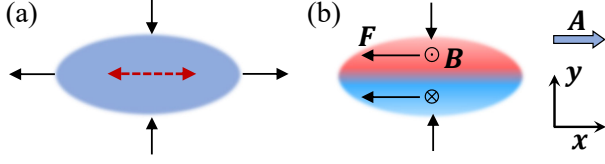


Figure 1. (a) Relevant collective modes of a BEC confined in a quasi-2D harmonic trap. The density-dependent gauge field is fixed in x direction, and couples the dipole oscillation in x direction (red dashed arrow) with breathing oscillations both in x and y directions (black arrow)(see Eq. 10). The dipole oscillation in y direction is decoupled in this scenario. (b) The Hall effect induced by the density-dependent gauge field. Red and Blue color denote the region where the effective magnetic field \mathbf{B} points to z and $-z$ directions, respectively. The breathing oscillation in y direction can induce a dipole oscillation in x direction and vice versa, through the Lorentz force \mathbf{F} .

II. VARIATIONAL WAVE FUNCTION METHOD

We start from the mean-field Hamiltonian which describes the atomic motion and atom-light coupling

$$\hat{H} = \left(\frac{\hat{\mathbf{p}}^2}{2m} + V(\mathbf{r}) \right) \otimes \mathbb{1} + H_{\text{int}} + U_{\text{AL}}, \quad (1)$$

where

$$U_{\text{AL}} = \frac{\hbar\Omega}{2} \begin{pmatrix} 0 & e^{-i\phi(\mathbf{r})} \\ e^{i\phi(\mathbf{r})} & 0 \end{pmatrix} \quad (2)$$

describes the coupling between two internal states $|1\rangle$ and $|2\rangle$, characterized by the two-photon Rabi frequency Ω and the laser phase $\phi(\mathbf{r})$. Here $V(\mathbf{r})$ is the external trap potential, $\mathbb{1}$ is the identity matrix defined in the pseudospin space spanned by $|1\rangle$ and $|2\rangle$, and $H_{\text{int}} = (1/2) \text{diag}[g_{11}\rho_1 + g_{12}\rho_2, g_{22}\rho_2 + g_{12}\rho_1]$ is the mean-field interaction characterized by two-body interaction strengths $g_{ll'} = 4\pi\hbar^2 a_{ll'}/m$, with $a_{ll'}$ being the scattering lengths for collisions between the components l and l' . The population of the i -th state is $\rho_i = |\Psi_i|^2$ ($i = 1, 2$).

For a dilute BEC, the coupling strength $\hbar\Omega$ is typically much larger than the mean-field energy. Therefore we can construct the interacting dressed states through perturbation theory with respect to the eigenstates of the atom-light coupling U_{AL} , namely, diagonalizing $U_{\text{AL}} + H_{\text{int}}$ by treating H_{int} as a small perturbation. We finally obtain the eigenstates of $U_{\text{AL}} + H_{\text{int}}$ represented by perturbed dressed states $|\chi_{\pm}\rangle = |\chi_{\pm}^{(0)}\rangle + |\chi_{\mp}^{(1)}\rangle$, where

$$|\chi_{\pm}^{(1)}\rangle = \pm \frac{g_{11} - g_{22}}{8\hbar} \rho_{\pm} |\chi_{\mp}^{(0)}\rangle, \quad (3)$$

with eigenvalues $g\rho_{\pm} \pm \hbar\Omega/2$. Here $g = (g_{11} + g_{22} + 2g_{12})/4$, $\rho_{\pm} = |\Psi_{\pm}|^2$ and the unperturbed dressed states $|\chi_{\pm}^{(0)}\rangle = (|1\rangle \pm \exp\{i\phi(\mathbf{r})\}|2\rangle)/\sqrt{2}$.

In order to derive an interacting gauge theory, we first expand a general state as $|\xi\rangle = \sum_{i=\{+,-\}} \Psi_i(\mathbf{r}, t) |\chi_i\rangle$. For atomic motion slow enough, we can make the adiabatic approximation and project the general wave function into one of the two dressed states, $|\chi_{\pm}\rangle$. The resulting effective Hamiltonian reads

$$\hat{H}_{\pm}^{\text{eff}} = \frac{1}{2m} (\hat{\mathbf{p}} - \mathbf{A}_{\pm})^2 + V(\mathbf{r}) + W \pm \frac{1}{2}\hbar\Omega + \frac{g}{2}\rho_{\pm}, \quad (4)$$

where a scalar potential $W = \hbar^2 |\langle \chi_{-} | \nabla \chi_{+} \rangle|^2 / 2m$ and a geometric vector potential $\mathbf{A}_{\pm} = i\hbar \langle \chi_{\pm} | \nabla \chi_{\pm} \rangle$ are introduced. According to aforementioned definition, the vector potential associated with the perturbed dressed state, to leading order, is given by

$$\mathbf{A}_{\pm} = \mathbf{A}^{(0)} \pm \mathbf{a}_1 |\Psi_{\pm}(\mathbf{r})|^2. \quad (5)$$

Here $\mathbf{A}^{(0)} = -(\hbar/2) \nabla \phi(\mathbf{r})$ is the single-particle vector potential and $\mathbf{a}_1 = (\nabla \phi(\mathbf{r})) (g_{11} - g_{22}) / (8\Omega)$ controls the effective strength of density-dependent vector potential. In the following we only consider one branch of the dressed states, e.g., the $+$ branch without loss of generality, and thus we can drop the \pm index in Eq. 4. Note that an effective magnetic field is associated with this density-dependent gauge field through $\mathbf{B} = \nabla \times \mathbf{A} = \nabla \rho \times \nabla \phi(\mathbf{r}) (g_{11} - g_{22}) / (8\Omega)$. So the density variation of BEC results in a non-vanishing density-dependent magnetic field, which is absent in the non-interacting case for the present setup. This effective magnetic field may induce a Hall effect, and has significant influence on the collective dynamics of BEC.

It was shown that BEC subject to this density-dependent gauge field obeyed a generalized Gross-Pitaevskii equation with current nonlinearity [15], and a variety of intriguing phenomena were predicted based on this equation [15, 31, 35]. Here we focus on the effect of this gauge field on the collective dynamics of BEC in a harmonic trap. Most studies on this topic usually consider a quasi-1D BEC, but as will be shown in the following, we find that the motion of a quasi-2D BEC is endowed with radically new physics. To illustrate this, we examined the dynamics of a quasi-2D BEC with motion in z direction frozen out. By using the method of variational wave function, the equation of motion is obtained by minimizing the Lagrangian

$$\mathcal{L} = \langle \Psi | i\hbar \partial_t - \hat{H}^{\text{eff}} | \Psi \rangle. \quad (6)$$

In particular, we choose a well-established variational wave function [37]

$$\Psi(\mathbf{r}, t) = f(z) C(t) \prod_{\eta=x,y} e^{-\frac{[\eta - \eta_0(t)]^2}{2w_{\eta}^2(t)} + i\eta\alpha_{\eta}(t) + i\eta^2\beta_{\eta}(t)}. \quad (7)$$

Here the harmonic potential is given by $V(\mathbf{r}) = (m\nu^2\lambda_x^2 x^2 + m\nu^2\lambda_y^2 y^2 + m\nu^2\lambda_z^2 z^2)/2$, with the quasi-2D condition $\lambda_z \gg \lambda_i$ ($i = x, y$). $f(z) = \exp[-z^2/(2a_z^2)]/(\sqrt{\pi}a_z)^{1/2}$ represents the BEC

wave function in z direction, with $a_z = [\hbar/(m\nu\lambda_z)]^{1/2}$ being the width of the Gaussian wave packet. The dynamical variables are the center of mass $\eta_0 = (x_0, y_0)$, amplitude $C(t)$, condensate width $w_\eta(t)$, slope $\alpha_\eta(t)$,

and variables related to curvature $\beta_\eta(t)$. Plugging the variational wave function $\Psi(\mathbf{r}, t)$ into Eq. 6 readily leads to the effective Lagrangian

$$\begin{aligned} \frac{\mathcal{L}}{N} = & \sum_{\eta=x,y} \left\{ \frac{\hbar}{2} (\dot{\beta}_\eta w_\eta^2 + 2\dot{\alpha}_\eta \eta_0 + 2\dot{\beta}_\eta \eta_0^2) + \frac{\hbar^2}{2m} \left[\frac{1}{2w_\eta^2} + \alpha_\eta^2 + 4\eta_0 \alpha_\eta \beta_\eta + 2(w_\eta^2 + 2\eta_0^2) \beta_\eta^2 \right] \right. \\ & - \left(\frac{\hbar}{m} A_\eta^{(0)} + \frac{N\hbar a_{1\eta}}{2\sqrt{2\pi^3} m a_z w_x w_y} \right) (\alpha_\eta + 2\eta_0 \beta_\eta) + \frac{1}{4} m \omega_\eta^2 (w_\eta^2 + 2\eta_0^2) \left. \right\} + \frac{\tilde{g}N}{4\sqrt{2\pi^3} a_z w_x w_y} \\ & + \frac{N^2 \mathbf{a}_{1\perp}^2}{6\sqrt{3} m \pi^3 a_z^2 w_x^2 w_y^2}, \end{aligned} \quad (8)$$

with $\tilde{g}/2 = g/2 + \mathbf{A}_\perp^{(0)} \cdot \mathbf{a}_{1\perp}/m$, $\mathbf{A}_\perp^{(0)} = (A_x^{(0)}, A_y^{(0)})$ and $\mathbf{a}_{1\perp} = (a_{1x}, a_{1y})$. The dot over the variable denotes time derivative of that variable. In terms of the notation $q_i \equiv \{w_x, w_y, x_0, y_0, \alpha_x, \alpha_y, \beta_x, \beta_y\}$, the Lagrangian equation reads

$$\frac{d}{dt} \left(\frac{\partial \mathcal{L}}{\partial \dot{q}_i} \right) - \frac{\partial \mathcal{L}}{\partial q_i} = 0, \quad (9)$$

from which one eventually arrives at the equations of motion of those dynamical variables.

For computational simplicity and without loss of generality, we assume the laser phase takes the form of a plane wave along x direction, namely, $\phi(\mathbf{r}) = kx$. Thus, the density-dependent gauge field is also along x direction. After introducing dimensionless variables and constants according to $\tau = \nu t$, $R_\eta = w_\eta/l_0$ ($\eta = x, y$), $R_z = a_z/l_0$, $P_x = k(g_{11} - g_{22})N/(8\Omega\hbar l_0^2)$, $P_y = 0$, and $G = gN/(\hbar\nu l_0^3)$, where $l_0 = [\hbar/(m\nu)]^{1/2}$, the resulting equations of motion finally read as follows:

$$\begin{aligned} \frac{d^2 \eta_0}{d\tau^2} + \lambda_\eta^2 \eta_0 &= \frac{P_\eta}{2\sqrt{2\pi^3} R_z R_x R_y} \sum_{\xi=x,y} \frac{1}{R_\xi} \frac{dR_\xi}{d\tau}, \\ \frac{d^2 R_\eta}{d\tau^2} + \lambda_\eta^2 R_\eta &= \frac{1}{R_\eta^3} + \left(\frac{2}{3\sqrt{3}} - \frac{1}{4} \right) \frac{P_x^2}{\pi^3 R_z^2 R_\eta R_x^2 R_y^2} \\ &+ \left(\frac{1}{2} G - P_x \frac{dx_0}{d\tau} \right) \frac{1}{\sqrt{2\pi^3} R_z R_\eta R_x R_y}. \end{aligned} \quad (10)$$

Note that the strength of the density-dependent gauge field is characterized by the dimensionless constant P_x .

In the absence of density-dependent gauge field, these equations describe the dipole and breathing modes of BEC [37], respectively. The dipole and breathing oscillations in x direction are always coupled, and for quasi-1D case, these are the only two relevant modes. For quasi-2D case, the gauge field also introduces a nontrivial coupling between the dipole mode in x direction and the breathing mode in y direction, reminiscent of the Hall effect induced by the gauge field, which is crucial for a comprehensive

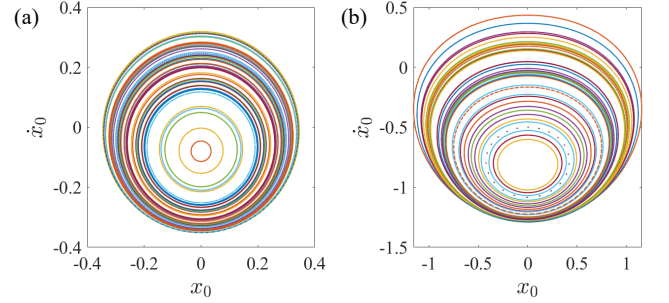


Figure 2. 2D Poincaré section of quasi-1D center of mass motion. Different color denotes different initial conditions. (a) $P_x = 0.5$, $E = 1.02 * E_{\min}$. (b) $P_x = 3$, $E = 1.2 * E_{\min}$. The other parameters are $R_y = 0.2$, $R_z = 0.2$, $\lambda_x = 1$, and $G = 5$.

description of the condensate dynamics. This coupling shows the key distinction between quasi-2D and quasi-1D cases, and plays an important role in the emergence of chaotic dynamics in quasi-2D case.

III. CHAOTIC DYNAMICS

Before solving the coupled nonlinear equations, we first note that the original Hamiltonian does not change with time, so the total energy is conserved,

$$\begin{aligned} \frac{E}{N} = & \frac{1}{4} \sum_{\eta=x,y} \left[\frac{1}{R_\eta^2} + \dot{R}_\eta^2 + 2\dot{\eta}_0^2 + \lambda_\eta^2 (R_\eta^2 + 2\eta_0^2) \right] \\ & + \frac{G}{4\sqrt{2\pi^3} R_z R_x R_y} + \frac{1}{4} \left(\frac{2}{3\sqrt{3}} - \frac{1}{4} \right) \frac{P_x^2}{\pi^3 R_z^2 R_x^2 R_y^2}, \end{aligned} \quad (11)$$

where an unimportant constant $W + \hbar\Omega/2$ is dropped out. Due to the conservation of total energy, when computing the Poincaré sections in the following, the total energy serves as a constrain for reducing the dimension of phase

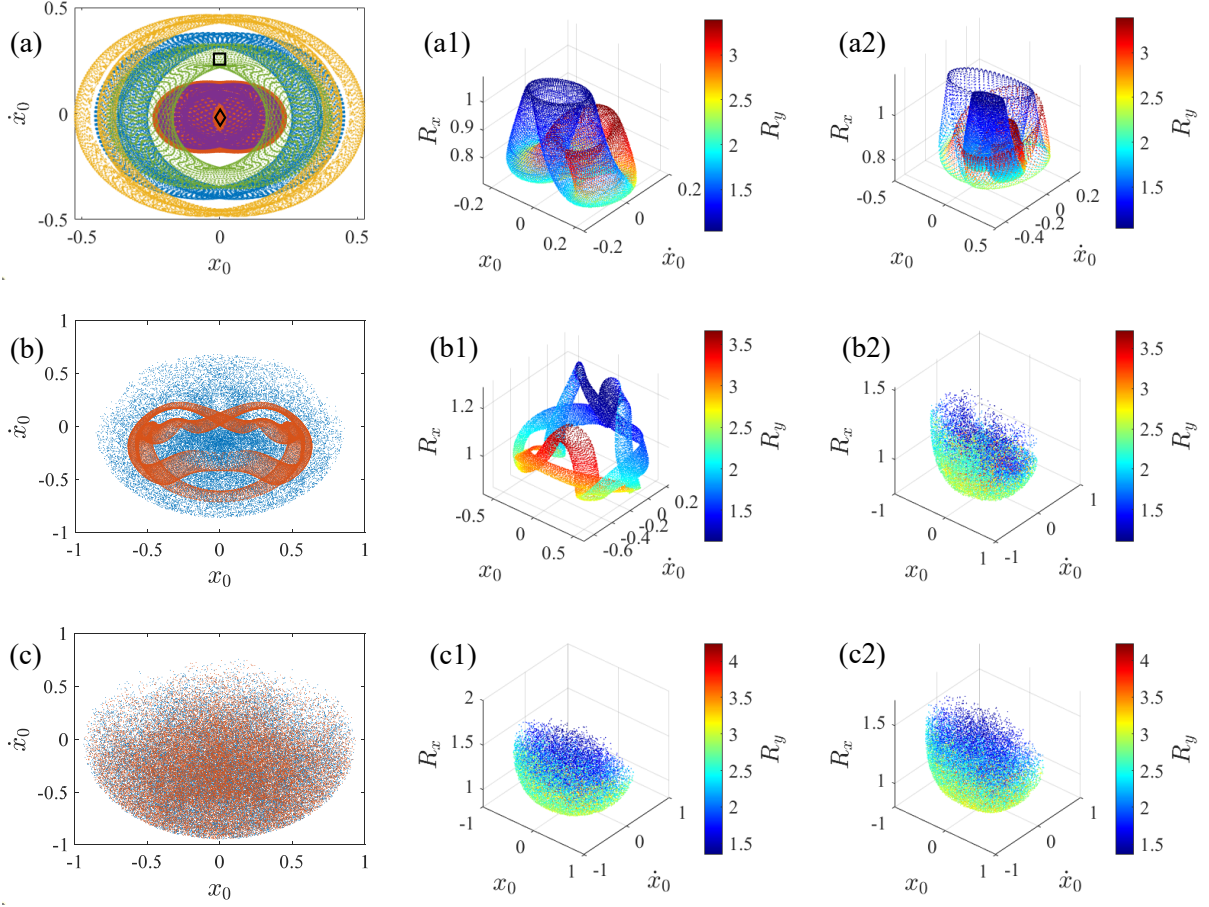


Figure 3. Projected 2D Poincaré section on the $x_0 - \dot{x}_0$ plane and 4D Poincaré section for certain orbits. (a) For weak density-dependent gauge field, only quasiperiodic orbits are present in Poincaré section. Different colors represent orbits with different initial conditions. The original 4D orbits for the central dark red curve (with diamond marker) and outer green curve (with square marker) are shown in (a1) and (a2), respectively. $P_x = 0.2$. (b) For moderate strength of gauge field, the phase space consists of quasiperiodic (dark red) and chaotic (dark blue) orbits, with their 4D form shown in (b1) and (b2), respectively. $P_x = 4$. (c) For strong gauge field, the Poincaré section consists of a chaotic sea, with scattered dark red and dark blue dots representing two chaotic orbits in (c1) and (c2) with different initial conditions. $P_x = 10$. The other parameters are $R_z = 0.2$, $\lambda_x = 1$, $\lambda_y = 0.5$, $G = 5$, and $E = 1.3 * E_{\min}$.

space. In addition, we first calculate the lowest energy E_{\min} at given parameters, and then use it as the energy unit.

For small amplitude oscillation, i.e., in the linear response regime, these equations can be linearized to give the frequency of coupled motion. To study oscillations of larger amplitude, or higher energy modes, one has to numerically solve these coupled equations to obtain the center of mass motion, along with the width motion of the condensate. The density-dependent gauge field couples these two kinds of motion, making the overall dynamics complicated. Here the spatial dimension of the underlying dynamics is crucial.

For comparison, we first consider the quasi-1D case. The condensate is tightly confined both in y and z directions, with their widths fixed to be the same $R_y = R_z$. The dynamical variables are then x_0 , \dot{x}_0 , R_x and \dot{R}_x . As the dimension of the phase space is four, by fixing the

total energy as well as another dynamical variable, e.g., $\dot{R}_x = 0$, we obtain a conventional 2D Poincaré section in the $x_0 - \dot{x}_0$ plane. The Poincaré section for two typical strengths of density-dependent gauge field is shown in Fig. 2. One sees that whether the density-dependent gauge field is weak (Fig. 2a) or strong (Fig. 2b), there are only regular dots and closed curves in the Poincaré section, corresponding to periodic and quasiperiodic orbits. These quasiperiodic motion may result from the irrational frequency ratio of dipole mode over breathing mode.

For the quasi-2D case, since the density-dependent gauge field has been fixed in x direction, the center of mass motion in y direction becomes decoupled, as evident from Eq. 10, and the remaining dynamical variables are x_0 , \dot{x}_0 , R_x , \dot{R}_x , R_y and \dot{R}_y . The phase space is six-dimensional, and thus by fixing the total energy along with $\dot{R}_x = 0$, the Poincaré section is four-dimensional.

In principle, one can also add two other constraints, e.g., by additionally fixing both R_x and R_y , to obtain a 2D Poincaré section, which however proves to be numerically quite challenging because of sparsity of those intersection points. In the present study, we use a 2D projection to illustrate the overall feature of the 4D Poincaré section, in conjunction with 4D visualization of certain orbits, similar to methods previously introduced elsewhere [36]. The 2D projection is on the $x_0 - \dot{x}_0$ plane, and the 4D visualization of certain orbits is achieved via a three-dimensional plot of x_0 , \dot{x}_0 , and R_x , with R_y represented by color.

Figure 3 shows the Poincaré section using the method described above, including its original 4D form and 2D projection on the $x_0 - \dot{x}_0$ plane. Only limited number of initial conditions are chosen in computing the Poincaré section, as those curves in projected 2D Poincaré section can overlap with each other, messing the Poincaré section for large number of initial conditions. This feature is in stark contrast with conventional 2D Poincaré section, where regular and chaotic orbits do not overlap with each other. When the density-dependent gauge field is weak, the projected 2D Poincaré section (Fig. 3a) consists of various distorted closed curves, which are originally distorted tori in the 4D Poincaré section (Fig. 3(a1),(a2)). So we conclude that these closed curves in projected 2D Poincaré section correspond to quasiperiodic orbits. Figure 3(a1) and (a2) show the original 4D Poincaré section for two different initial conditions, corresponding to the central dark red (with diamond marker) and outer green curves (with square marker) in Fig. 3a, respectively. With the increase of the strength of gauge field, chaotic orbits eventually appears, as shown by the scattered points in the chaotic sea of Fig. 3(b2), and its 2D projection in Fig. 3b (dark blue dots). Note that once the center of mass motion becomes chaotic, the motion of widths R_x and R_y are also chaotic. So one can also choose to project the 4D Poincaré on other 2D planes, and similar 2D chaotic sea will be observed. In this parameter regime, the Poincaré section consists of coexisting quasiperiodic (see Fig. 3(b1), corresponding to dark red dots in Fig. 3(b)) and chaotic orbits.

For sufficiently strong density-dependent gauge field, e.g., in the parameter regime shown in Fig. 3c, we only find chaotic orbits starting from various initial conditions. Figure 3(c1) and (c2) show the chaotic orbits with two different initial conditions in the 4D Poincaré section, with Fig. 3c being their 2D projections. The whole phase space in the Poincaré section is occupied by chaotic orbits. We also vary the strength of gauge field, total energy and trap anisotropy, and results show that stronger gauge field, higher energy and stronger trap anisotropy all favor the appearance of chaos in the collective motion of BEC.

To further confirm the nature of these chaotic orbits, we choose a typical initial condition in the chaotic sea of Fig. 3c, and show the time evolution as well as the power spectrum of one typical chaotic orbit in Fig. 4(b,d). The

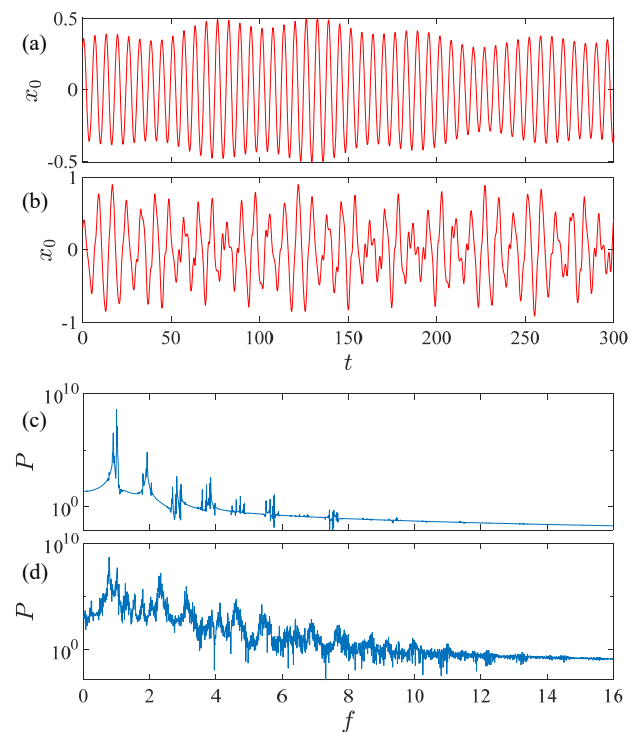


Figure 4. Quasiperiodic and chaotic dynamics of center of mass motion shown in time domain (a and b) and their power spectrums (c and d). (a) and (c) show the quasiperiodic motion, with $P_x = 0.2$. (b) and (d) show the chaotic motion, with $P_x = 10$. The frequency f is in the unit of $1/\nu$. The other parameters are $R_z = 0.2$, $\lambda_x = 1$, $\lambda_y = 0.5$, $G = 5$, and $E = 1.3 * E_{\min}$.

chaotic dynamics is manifested by the broad and structureless feature in power spectrum. For comparison, the time evolution and power spectrum of a typical quasiperiodic orbit is also shown in Fig. 4(a,c), with same parameters as Fig. 3a. The distinction between these two kinds of orbits is clear in both time evolution and power spectrum, consistent with our judgment based on Poincaré section.

The chaotic dynamics can be qualitatively understood as the interplay between three oscillations, namely, the dipole and breathing oscillations along the direction of gauge field, and the breathing oscillation in perpendicular direction. The former two modes are coupled through the current nonlinearity [15], while the dipole and breathing modes in perpendicular directions are coupled by the interaction induced Hall effect, only present for system of dimension two or higher. This explains the dramatic difference between quasi-1D and quasi-2D dynamics.

The major challenge towards the experimental observation of the chaotic dynamics of BEC predicted here is the relatively small difference between different scattering lengths, and therefore the density-dependent gauge field is relatively weak. Nevertheless, in principle one can employ the Feshbach resonance technique [38] to en-

hance the difference between different scattering lengths. The chaotic dynamics of BEC will be observed by measuring either the center of mass or the width motion of BEC in a harmonic trap.

IV. CONCLUSION

In summary, we have studied the effect of density-dependent gauge field on the collective dynamics of a harmonically trapped BEC. The center of mass dynamics depends sensitively on the spatial dimension of the condensate. For quasi-1D BEC, we only find quasiperiodic motion, whether the gauge field is weak or strong. In contrast, for quasi-2D BEC and strong gauge field, we find that the center of mass motion can become chaotic. This is also true for the dynamics of condensate width. The chaotic behavior are induced by the interplay between the dipole oscillation in the direction of gauge field and the breathing oscillations both along and perpendicular to that direction. The coupling between dipole and breathing oscillations in perpendicular direction can be understood as a Hall effect induced by the gauge field. We con-

firm the chaotic dynamics by computing the 4D Poincaré section, its projection on 2D plane, and the power spectrum. We find strong density-dependent gauge field, trap anisotropy and high energy are favorable for the observation of chaotic dynamics. Our findings deepen our understanding of the effect of dynamical gauge field in cold atomic gases, especially on the nonlinear dynamics of BEC.

V. ACKNOWLEDGMENTS

We thank Qiong-Tao Xie and Biao Wu for helpful discussions. L.C. is supported by the Science Foundation of Guizhou Science and Technology Department (Grants No. QKHJZ[2021]033 and No. QKHJZ[2018]1178), and the Science Foundation of Guizhou Provincial Education Department (Grant No. QJHKYZ[2017]087). Q.Z. is supported by the National Natural Science Foundation of China (Grant No. 12004118), the Guangdong Basic and Applied Basic Research Foundation (Grants No. 2020A1515110228 and No. 2021A1515010212), and the Science and Technology Program of Guangzhou (Grant No. 2019050001).

-
- [1] Y.-J. Lin, R. L. Compton, K. Jiménez-García, J. V. Porto, and I. B. Spielman, *Nature* **462**, 628 (2009).
 - [2] Y.-J. Lin, R. L. Compton, K. Jiménez-García, W. D. Phillips, J. V. Porto, and I. B. Spielman, *Nat. Phys.* **7**, 531 (2011).
 - [3] J. Dalibard, F. Gerbier, G. Juzeliūnas, and P. Öhberg, *Rev. Mod. Phys.* **83**, 1523 (2011).
 - [4] N. Goldman, G. Juzeliūnas, P. Öhberg, and I. B. Spielman, *Rep. Prog. Phys.* **77**, 126401 (2014).
 - [5] Y.-J. Lin, K. Jiménez-García, and I. B. Spielman, *Nature* **471**, 83 (2011).
 - [6] P. Wang, Z.-Q. Yu, Z. Fu, J. Miao, L. Huang, S. Chai, H. Zhai, and J. Zhang, *Phys. Rev. Lett.* **109**, 095301 (2012).
 - [7] L. W. Cheuk, A. T. Sommer, Z. Hadzibabic, T. Yefsah, W. S. Bakr, and M. W. Zwierlein, *Phys. Rev. Lett.* **109**, 095302 (2012).
 - [8] H. Zhai, *Rep. Prog. Phys.* **78**, 026001 (2015).
 - [9] L. Huang, Z. Meng, P. Wang, P. Peng, S.-L. Zhang, L. Chen, D. Li, Q. Zhou, and J. Zhang, *Nat. Phys.* **12**, 540 (2016).
 - [10] Z. Wu, L. Zhang, W. Sun, X.-T. Xu, B.-Z. Wang, S.-C. Ji, Y. Deng, S. Chen, X.-J. Liu, and J.-W. Pan, *Science* **354**, 83 (2016).
 - [11] T. Keilmann, S. Lanzmich, I. McCulloch, and M. Roncaglia, *Nat. Commun.* **2**, 361 (2011).
 - [12] D. Banerjee, M. Dalmonte, M. Müller, E. Rico, P. Stebler, U.-J. Wiese, and P. Zoller, *Phys. Rev. Lett.* **109**, 175302 (2012).
 - [13] E. Zohar, J. I. Cirac, and B. Reznik, *Phys. Rev. Lett.* **110**, 125304 (2013).
 - [14] L. Tagliacozzo, A. Celi, P. Orland, M. W. Mitchell, and M. Lewenstein, *Nat. Commun.* **4**, 2615 (2013).
 - [15] M. J. Edmonds, M. Valiente, G. Juzeliūnas, L. Santos, and P. Öhberg, *Phys. Rev. Lett.* **110**, 085301 (2013).
 - [16] S. Greschner, G. Sun, D. Poletti, and L. Santos, *Phys. Rev. Lett.* **113**, 215303 (2014).
 - [17] K. E. Ballantine, B. L. Lev, and J. Keeling, *Phys. Rev. Lett.* **118**, 045302 (2017).
 - [18] L. W. Clark, B. M. Anderson, L. Feng, A. Gaj, K. Levin, and C. Chin, *Phys. Rev. Lett.* **121**, 030402 (2018).
 - [19] C. Schweizer, F. Grusdt, M. Berngruber, L. Barbiero, E. Demler, N. Goldman, I. Bloch, and M. Aidelsburger, *Nat. Phys.* **15**, 1168 (2019).
 - [20] F. Görg, K. Sandholzer, J. Minguzzi, R. Desbuquois, M. Messer, and T. Esslinger, *Nat. Phys.* **15**, 1161 (2019).
 - [21] R. M. Kroeze, Y. Guo, and B. L. Lev, *Phys. Rev. Lett.* **123**, 160404 (2019).
 - [22] P. Xu, T.-S. Deng, W. Zheng, and H. Zhai, *Phys. Rev. A* **103**, L061302 (2021).
 - [23] L. Dong, L. Zhou, B. Wu, B. Ramachandhran, and H. Pu, *Phys. Rev. A* **89**, 011602 (2014).
 - [24] J.-h. Zheng, B. Xiong, G. Juzeliūnas, and D.-W. Wang, *Phys. Rev. A* **92**, 013604 (2015).
 - [25] D. Raventós, T. Graß, B. Juliá-Díaz, L. Santos, and M. Lewenstein, *Phys. Rev. A* **93**, 033605 (2016).
 - [26] W. Zheng and N. R. Cooper, *Phys. Rev. Lett.* **117**, 175302 (2016).
 - [27] Z. Yao, C. Liu, P. Zhang, and H. Zhai, *Phys. Rev. B* **102**, 104302 (2020).
 - [28] S.-L. Zhu, H. Fu, C.-J. Wu, S.-C. Zhang, and L.-M. Duan, *Phys. Rev. Lett.* **97**, 240401 (2006).
 - [29] L. J. LeBlanc, K. Jiménez-García, R. A. Williams, M. C. Beeler, A. R. Perry, W. D. Phillips, and I. B. Spielman, *PNAS* **109**, 10811 (2012).

- [30] J.-y. Choi, S. Kang, S. W. Seo, W. J. Kwon, and Y.-i. Shin, Phys. Rev. Lett. **111**, 245301 (2013).
- [31] M. J. Edmonds, M. Valiente, and P. Öhberg, EPL **110**, 36004 (2015).
- [32] R. J. Dingwall, M. J. Edmonds, J. L. Helm, B. A. Malomed, and P. Öhberg, New J. Phys. **20**, 043004 (2018).
- [33] R. J. Dingwall and P. Öhberg, Phys. Rev. A **99**, 023609 (2019).
- [34] S. Butera, M. Valiente, and P. Öhberg, New J. Phys. **18**, 085001 (2016).
- [35] M. Edmonds and M. Nitta, Phys. Rev. A **102**, 011303 (2020).
- [36] G. Lukes-Gerakopoulos, M. Katsanikas, P. A. Patsis, and J. Seyrich, Phys. Rev. D **94**, 024024 (2016).
- [37] V. M. Pérez-García, H. Michinel, J. I. Cirac, M. Lewenstein, and P. Zoller, Phys. Rev. Lett. **77**, 5320 (1996).
- [38] C. Chin, R. Grimm, P. Julienne, and E. Tiesinga, Rev. Mod. Phys. **82**, 1225 (2010).